



Tailored disorder: a self-organized photonic contact for light trapping in silicon-based tandem solar cells

HUBERT HAUSER,¹ KAI MÜHLBACH,¹ OLIVER HÖHN,¹ RALPH MÜLLER,¹ SONJA SEITZ,¹ JÜRGEN RÜHE,² STEFAN W. GLUNZ,^{1,3} AND BENEDIKT BLÄSI^{1,*}

¹Fraunhofer Institute for Solar Energy Systems (ISE), Heidenhofstrasse 2, D-79110 Freiburg, Germany

²Department of Microsystems Engineering (IMTEK), University of Freiburg, Freiburg, Germany

³Laboratory for Photovoltaic Energy Conversion, University of Freiburg, 79110 Freiburg, Germany

*benedikt.blasi@ise.fraunhofer.de

Abstract: We present a process development leading to efficient rear side light trapping structures with the purpose of enhancing the infrared response of a silicon-based tandem solar cell. To this end, we make use of phase separation effects of two immiscible polymers, polystyrene and poly(methyl methacrylate), resulting in a non-periodic polystyrene structure on silicon with a well-defined size distribution. Onto this pattern, we evaporate silver as a scattering rear side mirror and contact layer. Average feature sizes and periods can be tuned by varying material properties (e.g. molar weights or ratios of the polymers) as well as processing conditions during the spin coating. This way a favorable pseudo period of approx. 1 μm for these disordered structure features was realized and successfully implemented into a silicon solar cell. The structure shows a ring-shaped scattering distribution which is beneficial for light trapping in solar cells. External quantum efficiency measurements show that a gain in short circuit current density of 1.1 mA/cm² compared to a planar reference can be achieved, which is in the same range as we achieved using nanoimprint lithography in a record triple-junction III/V on a silicon device.

© 2020 Optical Society of America under the terms of the [OSA Open Access Publishing Agreement](#)

1. Introduction

In silicon solar cells measures to enhance light incoupling as well as internal pathlengths are commonly applied in terms of surface textures. State-of-the-art textures are pyramidal textures on monocrystalline silicon [1] and the so-called isotexture on multicrystalline silicon [2]. As single-junction silicon solar cells are more and more approaching theoretical limit of 29.4% in their conversion efficiency [3,4], multi-junction solar cell architectures using silicon as bottom cell material are currently a major field of research. Promising candidates as top cell material are III-V semiconductors [5,6] or perovskites [7]. The near infrared response of silicon, as an indirect semiconductor, can be improved significantly by tailored photon management [8]. Such photon management concepts are especially attractive for highest efficiency devices, such as silicon based multi-junction solar cells.

Depending on the top cell material and joining process of the sub-cells, restrictions can arise that hinder the realization of surface textures. In III-V on silicon tandem cells one approach to join sub-cells is direct wafer bonding. This delicate process requires perfectly polished surfaces and thus is not compatible with textured surfaces [9,10]. Another restriction can be the passivation quality of the silicon bottom cell. For example, for passivated contacts in p-type silicon, it is known that a texture leads to a less effective surface passivation [11]. Therefore, in [5] a III-V // silicon multi-junction solar cell with planar silicon interfaces incorporating passivated contacts on both sides was realized using direct wafer bonding. However, it was found that without any additional measures the IR response of the silicon bottom cell was moderate as it can be expected.

With the aim of introducing a photonic light trapping structure, there, a polymeric diffraction grating with a period of $1\text{ }\mu\text{m}$ was realized using Roller-Nanoimprint Lithography (Roller-NIL) [12,13]. This grating was partially opened and coated with silver acting as photonic mirror and rear side contact at the same time (photonic contact). This rear side structure led to a gain in J_{sc} of 1.2 mA/cm^2 and thus to an efficiency gain of 1.9% absolute.

This result is in accordance with earlier design studies as well as experimental results showing that gratings with a period around $1\text{ }\mu\text{m}$ are very well suited for crystalline silicon solar cells (single-junction as well as bottom cells in tandem devices) [8,14–17]. More generally, for optically thick absorber materials it is a good choice if the period is in the same range as the wavelengths for which light trapping shall be achieved.

Besides periodic gratings, non-periodic photonic structures were investigated as light trapping structures in solar cells. For thin film solar cells, stochastic structures were investigated and are commercially applied in order to achieve strong scattering and high haze values, see e.g. [18–20]. For this application, also “deterministic quasi-random” structures [21] or structures with tailored Power Spectral Density (PSD) [22] were investigated, aiming for a ring shaped PSD, resulting in a ring shaped scattering profile. Such structures lead to very good light trapping due to a strong path length enhancement and minimized direct outcoupling. Other authors chose an approach in the other direction, introducing complex supercells [23] or disorder into regular structures [24]. In more recent work, the term “tailored disorder” was used for such structures with defined irregularities [25,26].

One way to fabricate structures featuring tailored disorder is based on the phase separation of immiscible polymers [27,28]. The driving force of the phase separation is the different polarity of polymers as e.g. for polystyrene (PS) and poly(methyl methacrylate) (PMMA). The two polymers are mixed in a solvent and are applied to a substrate via spin coating. During the spin coating process the solvent evaporates, leading to the phase separation and leaving behind a non-periodic arrangement of the two polymer phases. By adjusting parameters like molecular weights and ratios of the polymers, pattern characteristics as e.g. mean feature size or PSD can be tuned [29].

Such phase separation processes were used to fabricate light trapping structures for thin film solar cells [30], leading to a substantial external quantum efficiency (EQE) enhancement on a rather low absolute efficiency level [31]. Here, we apply a similar process chain to wafer-based high efficiency silicon solar cells with passivated contacts on front and rear. These solar cells have due their high passivation quality highest voltages and thus are extremely sensitive to any introduction of smallest defects. This makes the successful implementation of light trapping structures without deterioration of other cell parameters extremely challenging.

In accordance with the above referenced literature on deterministic quasi-random structures or tailored disorder (e.g. [22,25]), the aforementioned design rule for gratings can be generalized to non-periodic structures: The maximum in the PSD should correspond to the wavelength range for which light trapping shall be achieved, which we can achieve via a self-organized photonic contact.

2. Experiment

2.1. Phase separation process

There are different material combinations of polymers and solvents suitable for the application in a self-organized de-mixing process. An overview of suitable materials can be found in Ref. [32]. A simple fabrication sketch is shown in Fig. 1.

We chose the well-investigated material combination of PS and PMMA as the two immiscible polymers of different polarity [28,29]. Methylethylketone (MEK) was chosen as solvent for being capable of dissolving both polymers. A blend of the two polymers in MEK is then applied via spin coating. After the phase separation process occurring during the spin coating process and the evaporation of the solvent, we dissolved the PMMA polymer phase in acetic acid leaving

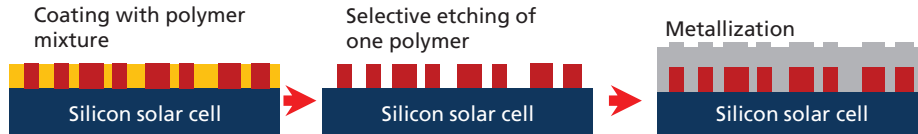


Fig. 1. Simple sketch of the phase separation process (according to [33]). We used the polymers PMMA (orange) and PS (red), resulting in a PS structure after dissolving the PMMA. Details on possible process parameters and their effect can be found in [32]. As last step, silver was evaporated in order to form the contact and enhance reflection.

behind a PS pattern on the silicon surface. Table 1 summarizes the main material and blend parameters investigated within this study.

Table 1. Overview of the main material and blend parameters varied within this study.

PMMA MW [kg/mol]	PS MW [kg/mol]	Mixing ratio PMMA : PS	Polymer content [wt. %]	Spin speed [rpm]
15, 120, 320	35, 192, 280	3:1-1:3	1.9 - 7	750-5000

Varying these parameters, we aimed for a homogeneous coverage of structure features with a well-defined spatial frequency distribution. It has to be emphasized that the dependency of the resulting structure properties on the processing conditions and parameters is very complex. The investigation of major trends can be found in [32]. As described before, it has been shown that for periodic features a period of 1 μm is beneficial for silicon-based solar cells [8,14-17]. Therefore, we aimed for structures with a similar corresponding PSD. For solar cells made of other semiconductors (e.g. GaAs) of course this ideal period (or typical feature size) will change as optimum light trapping has to be realized for photons close to the band gap energy.

2.2. Solar cell fabrication

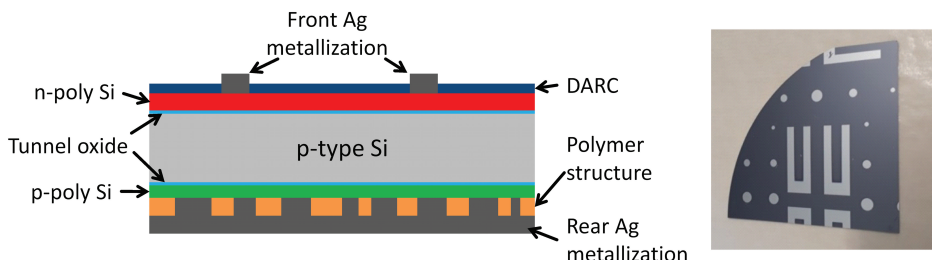


Fig. 2. Left: Sketch of the solar cell structure applied within this work. On the rear side of a p-type wafer with polysilicon passivated contacts on front (n-type) and rear (p-type) a polymer structure is applied onto which the rear side Ag metallization is deposited (self-organized photonic contact). Right: A photograph showing the Ag front side contacts for these test devices realized using evaporation through a shadow mask.

We fabricated solar cells specially designed for their use as bottom solar cells, which are very similar to the ones applied in Ref. [5]. However, the cells were realized in a leaner process flow with the silver front contact being evaporated through a shadow mask. The front contact geometry with large spacing was used in order to evaluate the EQE without shadowing effects as well as Suns-V_{oc} characterization [34] of the samples in order to proof that the extremely high

cell quality is not affected by the structuring process; a standard IV-characterization was not purpose of this work.

We used 280 μm thick planar FZ p-type 1-5 $\Omega\text{ cm}$ wafers, which were coated with a 100 nm thick polysilicon layer using LPCVD on both sides (n-doped on the front, p-doped on the rear) on a thin tunnel oxide (TOPCon structure). More details on the solar cell fabrication can be found in Ref. [5] and [35]. On the planar front a double layer anti-reflection coating (DARC) consisting of 55 nm TiO_2 and 110 nm MgF_2 was deposited (very similar to the one applied in [5]). Using the phase separation process described before, on the rear side of the solar cells, PS structures were realized leaving the polysilicon surface partially opened for the latter metallization. After subsequently removing the native oxide layer in an HF-dip, a 1 μm thick silver reflector was evaporated onto the rear side with polymer structures. As a result of this processing sequence a self-organized photonic contact is realized on the rear side. The solar cell structure as well as the geometry of the front contacts designed for these single junction test devices is shown in Fig. 2.

3. Results and discussion

3.1. Topography

Table 2. Exemplary material and process parameters applied for the samples to study topography and optical effects.

Sample	PMMA MW [kg/mol]	PS MW [kg/mol]	Mixing ratio PMMA : PS	Polymer content [wt. %]	Spin speed [rpm]
#1	15k	35k	1:1	4	1500
#2	15k	35k	3:2	2	1500

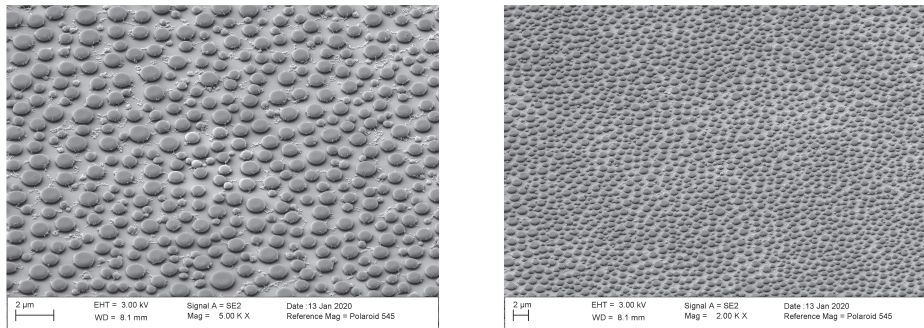


Fig. 3. SEM micrographs of the same sample (type #1) with different magnification showing the homogeneous distribution of the PS structures on a silicon substrate. The tilt angle in these micrographs is 67°.

The structural characterization was done by Scanning Electron Microscopy (SEM) and Atomic Force Microscopy (AFM). While the SEM micrograph allows a good qualitative evaluation of profile shapes and homogeneity, the AFM scans can be used to extract quantitative parameters. The AFM measurements were performed with a Bruker Dimension Edge in tapping mode with Tap 300 cantilevers. In this study of topographical results and the characterization thereof, we exemplarily show two types of samples to visualize the tunability of the process as well as the resulting narrow size distribution allowing for photonic effects. The fabrication parameters of these two sample sets are summarized in Table 2.

In Fig. 3 SEM micrographs of sample type #1 are shown for the resulting PS polymer pattern on a silicon wafer. It already can be seen that the coverage is quite homogeneous and the size distribution is rather narrow.

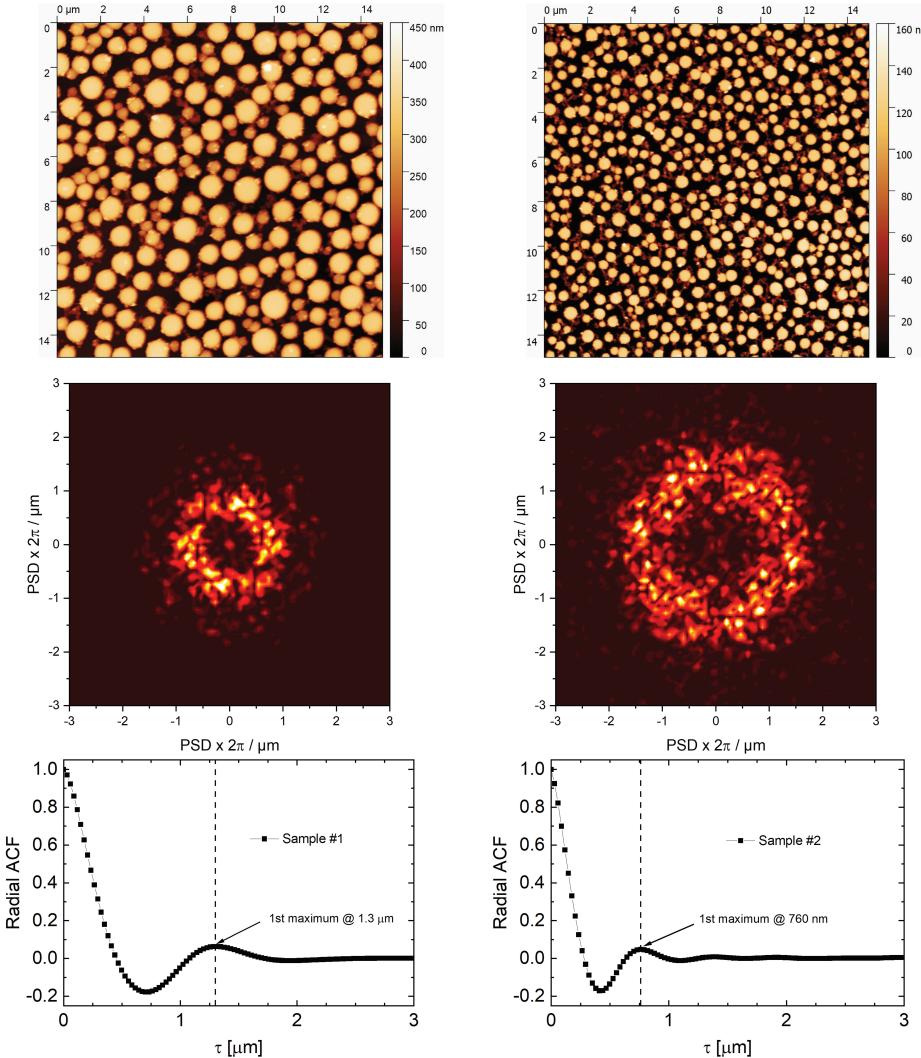


Fig. 4. AFM micrographs (top row) as well as 2D PSD (middle row) and radial ACF (bottom row) determined from these graphs. Left column: PS structure #1 with a pseudo period of $1.3 \mu m$ and a pattern depth of $310 nm$. Right column: PS structure #2 with a pseudo period of $760 nm$ and a pattern depth of $120 nm$.

The AFM characterization allows the extraction of the parameters depth, autocorrelation function (ACF), pseudo period and PSD. This post-processing of the AFM micrographs was done using the software Gwyddion [36]. As a key structure parameter, the pseudo period within this work is defined as the first value $> 0 \mu m$, for which the radial ACF assumes a relative maximum (see Fig. 4, bottom row). So for a periodic grating, period and pseudo period would be the same. This analogy is very instructive since period and pseudo period define predominant diffraction/scattering angles. This analysis leads to a pseudo period of $1.3 \mu m$ of these PS features

for sample type #1. Thus, we successfully realized features arranged in tailored disorder with a slightly larger pseudo period than specified above for the application as light trapping structures in silicon solar cells. The AFM analysis of sample type #2 yields a pseudo period of 760 nm. This structure would be well suited as light trapping structure for photons with energies close to the band gap in a GaAs solar cell. In Fig. 4 (left) the AFM profile scans for the two structures are displayed, while in the right column the 2D PSD is shown. The PSD plots show nicely the ring shaped distributions which have maxima at spatial frequencies lower than $2\pi/\mu\text{m}$, corresponding to a pseudo period $> 1 \mu\text{m}$ (#1), and higher than $2\pi/\mu\text{m}$, corresponding to a pseudo period $< 1 \mu\text{m}$ (#2).

3.2. Optical analysis

A fast and effective method to characterize the structured samples regarding their pattern quality, pseudo period and thus potential optical light trapping properties is the recording of a scattering or diffraction profile, as already shown in Ref. [22]. To do so, we took a photograph of the reflected light distribution of a HeNe-laser ($\lambda = 633 \text{ nm}$) interacting with the PS polymer pattern on a silicon wafer (sample type #1, see Fig. 5, left). It can be seen that the scattering profile on the screen has a ring shape with a depletion zone around the direct specular reflection. This behavior highlights that there is a defined size and pitch distribution as the features do not lead to a Gaussian type of scattering but also include a diffractive behavior leading to this ring shape.

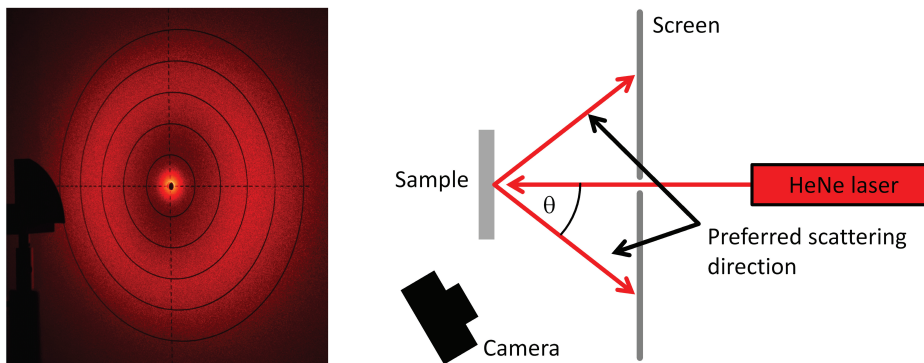


Fig. 5. Left: Photograph of the ring-shaped reflection pattern of a HeNe-laser beam interacting with the sample type #1 PS pattern on a silicon wafer. The concentric circles on the screen have a distance of 2.5 cm. Since the photograph is taken from an angle, the image shows an elliptic projection. Right: Sketch of the setup for taking this photograph.

Measuring the radius of the ring (maximum intensity) and the distance of the sample to the screen, allows the calculation of the pseudo period Λ from the scattering angle θ using the diffraction grating equation $\Lambda = \lambda / (\sin \theta)$. In this case, a mean radius of the ring of 8 cm and a distance of sample to diffusor of 15 cm ($\theta = 28^\circ$) leads to a pseudo period of $1.35 \mu\text{m}$. Taking the AFM micrograph of the corresponding sample shown in Fig. 4 (top left), the ACF can be extracted (Fig. 4, bottom left). It is important to note that the ACF is another way to express the data shown above in the PSD, with a Fourier's transformation being the mathematical operation. The first maximum of the ACF lies at $1.3 \mu\text{m}$ which is in very good agreement with the pseudo period deduced from the ring shaped scattering distribution.

3.3. Solar cell performance

The performance of the self-organized photonic contact in terms of light trapping was determined in external quantum efficiency (EQE) measurements. To this end, silicon solar cells were

fabricated with varying parameters for the polymeric structure on the rear side. The sample set comprised of two planar references (silver directly on the planar rear) and eight patterned cells (two for each parameter set). We realized PS features with pseudo periods ranging from 1.1 to 2.6 μm . The resulting current density gain compared to the planar reference lies between 0.3 and 1.1 mA/cm^2 and was highest for the smallest pseudo period. Thus, all blends led to an enhanced response in the near IR range compared to the planar reference. In the following, the characterization of the best sample is described in detail. It is important to state that the solar cell samples were processed in a different laboratory (clean room) and using a different spin coater (different solvent atmosphere during spin coating). Different laboratory conditions (temperature, humidity) as well as a different set up for the spin coating process are influencing the resulting topography. Therefore, it can be expected that the parameter study we performed before cannot be transferred directly. The set of parameters applied for the best cell is summarized in Table 3.

Table 3. Material and processing parameters applied for the best solar cell. Spin coater and processing environment (clean room) differ from the samples in sections 3.1 and 3.2. So the parameters are not directly comparable.

Sample	PMMA MW [kg/mol]	PS MW [kg/mol]	Mixing ratio PMMA : PS	Polymer content [wt. %]	Spin speed [rpm]
Best Cell	15k	35k	3:2	4	3000

Prior to the silver evaporation, the PS pattern on the rear side of the solar cell was characterized using the AFM and the PSD was extracted (see Fig. 6). From this data a pseudo period of 1.1 μm was calculated. This again fits very well to the targeted light trapping structure for silicon solar cells with a period around 1 μm .

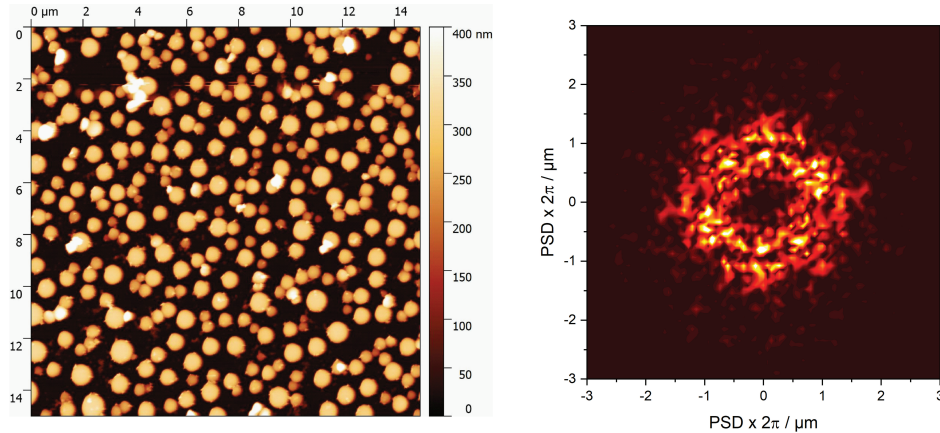


Fig. 6. AFM micrograph as well as the PSD for the best solar cell processed using the parameters described in Table 3. The corresponding pseudo period is 1.1 μm .

Figure 7 shows EQE measurements of this best material / process combination as well as a planar reference. The J_{sc} can be calculated from EQE measurements via

$$J_{sc} = q \cdot \int EQE(\lambda) \cdot \Phi_{AM1.5g}(\lambda) d\lambda \quad (1)$$

with $\Phi_{AM1.5g}$ being the photon flux of the AM1.5g solar spectrum [37] and q being the elementary charge. An integration of the EQE enhancement compared to the planar reference corresponds to a gain in J_{sc} of 1.1 mA/cm^2 (hatched area in Fig. 7). Besides EQE measurements, we also

characterized the samples by means of Suns-V_{oc} measurements [34]. Both, EQE and Suns-V_{oc} measurements have been conducted for one sun illumination. The two planar references showed V_{oc} values of 687 mV and 682 mV. The six solar cells with polymeric rear showed a mean V_{oc} of 686 mV with a standard deviation of 4.4 mV. Thus, we did not see any detrimental influence of the additional polymer structure on the passivation quality. This finally proves that the developed process does not influence the excellent and thus highly sensitive passivation quality. It can be concluded that this process is suitable for the improvement of highest efficiency solar cells.

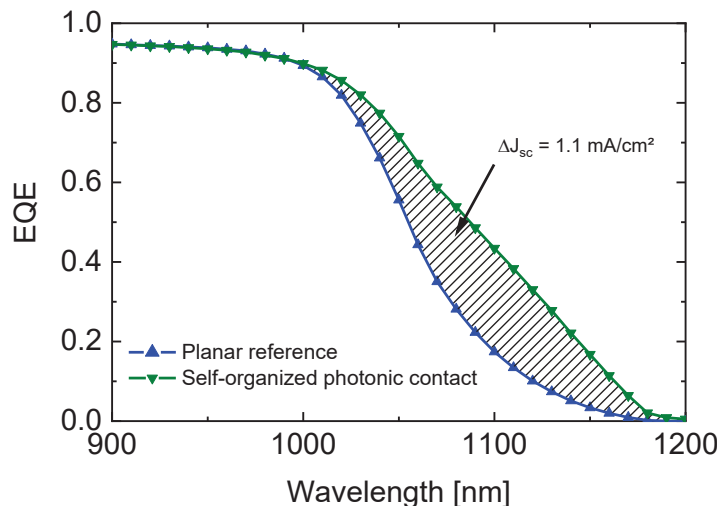


Fig. 7. EQE measurements of a planar reference sample (blue), as well as a solar cell with a self-organized photonic contact on the rear side (green). The hatched area indicates the gain in J_{sc} and an integration using Eq. (1) leads to 1.1 mA/cm².

It can be concluded that the self-organized photonic contact described within this work shows a comparable enhancement in J_{sc} as reached with a periodic grating using NIL. It has been shown that there is no degradation in terms of electrical properties. However, the presented process chain based on the self-organization does not rely on a template-based process as for NIL, where the stamping itself as well as the degradation of stamps goes in hand with expenses and efforts. In the current study we investigated spin coating as process technique to apply the polymer blend; however, it has been shown that scaleable techniques like dip coating [38] or slot die coating [39] are also feasible for the deposition of polymer blend solutions. Thus, we presented a processing scheme simplifying the realization of photonic structures in silicon-based tandem devices.

4. Conclusions and outlook

In this work, we realized a self-organized photonic contact on the rear of silicon bottom solar cells. To this end, we applied phase separation of two immiscible polymers (PS and PMMA) to achieve a stochastical arrangement of PS features with a narrow size and pitch distribution. In agreement to literature, we found that this so-called pseudo period can be tuned by modifying material, blend and process parameters. This way, we were able to fine tune resulting pseudo periods to achieve well suited structure parameters for their use as light trapping structures in silicon (pseudo period of 1.1 μm) or also e.g. GaAs (pseudo period of 760 nm) solar cells.

It is shown that it is possible to integrate the polymer phase separation process into a process flow to fabricate silicon solar cells. An improvement of the near IR response of planar silicon solar cells is demonstrated, as they e.g. are used in III/V on silicon multi-junction cells [5]. This

EQE enhancement corresponds to a gain in the short circuit current density of 1.1 mA/cm^2 . This gain is on a comparable level as we have shown for a very similar concept of a photonic contact based on strictly periodic polymeric features (1.2 mA/cm^2) [5]. However, the bottom-up process presented in this work requires one process step less than the top-down NIL approach and avoids issues like e.g. stamp degradation. In a next step, we will investigate the integration of such a simple self-organized photonic contact in a silicon-based multi-junction solar cell.

Funding

Horizon 2020 Framework Programme (project SiTaSol, 727497).

Acknowledgments

The authors would like to thank Volker Kübler, Christine Wellens and Felix Schätzle at Fraunhofer ISE for their support. We also thank the European Union's Horizon 2020 research and innovation programme within the project SiTaSol.

Disclosures

The authors declare no conflicts of interest.

References

1. P. Campbell and M. A. Green, "Light trapping properties of pyramidal textured surfaces," *J. Appl. Phys.* **62**(1), 243–249 (1987).
2. A. Hauser, I. Melnyk, P. Fath, S. Narayanan, S. Roberts, and T. M. Bruton, "A simplified process for isotropic texturing of mc-Si," in *Proceedings of the 3rd World Conference on Photovoltaic Energy Conversion* (2003), pp. 1447–1450.
3. A. Richter, M. Hermle, and S. W. Glunz, "Reassessment of the limiting efficiency for crystalline silicon solar cells," *IEEE J. Photovolt.* **3**(4), 1184–1191 (2013).
4. K. Yoshikawa, H. Kawasaki, W. Yoshida, T. Irie, K. Konishi, K. Nakano, T. Uto, D. Adachi, M. Kanematsu, H. Uzu, and K. Yamamoto, "Silicon heterojunction solar cell with interdigitated back contacts for a photoconversion efficiency over 26%," *Nat. Energy* **2**(5), 17032 (2017).
5. R. Cariou, J. Benick, F. Feldmann, O. Höhn, H. Hauser, P. Beutel, N. Razek, M. Wimplinger, B. Bläsi, D. Lackner, M. Hermle, G. Siefer, S. W. Glunz, A. W. Bett, and F. Dimroth, "III–V-on-silicon solar cells reaching 33% photoconversion efficiency in two-terminal configuration," *Nat. Energy* **3**(4), 326–333 (2018).
6. S. Essig, C. Allebé, T. Remo, J. F. Geisz, M. A. Steiner, K. Horowitz, L. Barraud, J. S. Ward, M. Schnabel, A. Descocedres, D. L. Young, M. Woodhouse, M. Despesse, C. Ballif, and A. Tamboli, "Raising the one-sun conversion efficiency of III–V/Si solar cells to 32.8% for two junctions and 35.9% for three junctions," *Nat. Energy* **2**(9), 17144 (2017).
7. K. A. Bush, A. F. Palmstrom, Z. J. Yu, M. Boccard, R. Checharoen, J. P. Mailoa, D. P. McMeekin, R. L. Z. Hoye, C. D. Bailie, T. Leijtens, I. M. Peters, M. C. Minichetti, N. Rolston, R. Prasanna, S. Sofia, D. Harwood, W. Ma, F. Moghadam, H. J. Snaith, T. Buonassisi, Z. C. Holman, S. F. Bent, and M. D. McGehee, "23.6%-efficient monolithic perovskite/silicon tandem solar cells with improved stability," *Nat. Energy* **2**(4), 17009 (2017).
8. J. Eisenlohr, N. Tucher, H. Hauser, M. Graf, J. Benick, B. Bläsi, J. C. Goldschmidt, and M. Hermle, "Efficiency increase of crystalline silicon solar cells with nanoimprinted rear side gratings for enhanced light trapping," *Sol. Energy Mater. Sol. Cells* **155**, 288–293 (2016).
9. R. Cariou, J. Benick, P. Beutel, N. Razek, C. Flotgen, M. Hermle, D. Lackner, S. W. Glunz, A. W. Bett, M. Wimplinger, and F. Dimroth, "Monolithic Two-Terminal III–V//Si Triple-Junction Solar Cells With 30.2% Efficiency Under 1-Sun AM1.5 g," *IEEE J. Photovolt.* **7**(1), 367–373 (2017).
10. S. Essig, J. Benick, M. Schachtner, A. Wekkeli, M. Hermle, and F. Dimroth, "Wafer-Bonded GaInP/GaAs//Si Solar Cells With 30% Efficiency Under Concentrated Sunlight," *IEEE J. Photovolt.* **5**(3), 977–981 (2015).
11. Y. Larionova, M. Turcu, S. Reiter, R. Brendel, D. Tetzlaff, J. Krügener, T. Wietler, U. Höhne, J.-D. Kähler, and R. Peibst, "On the recombination behavior of p + -type polysilicon on oxide junctions deposited by different methods on textured and planar surfaces," *Phys. Status Solidi A* **214**(8), 1700058 (2017).
12. H. Hauser, B. Michl, S. Schwarzkopf, V. Kübler, C. Müller, M. Hermle, and B. Bläsi, "Honeycomb texturing of Silicon via nanoimprint lithography for solar cell applications," *IEEE J. Photovolt.* **2**(2), 114–122 (2012).
13. N. Tucher, O. Höhn, H. Hauser, C. Müller, and B. Bläsi, "Characterizing the degradation of PDMS stamps in nanoimprint lithography," *Microelectron. Eng.* **180**, 40–44 (2017).

14. J. Eisenlohr, B. G. Lee, J. Benick, F. Feldmann, M. Drießen, N. Milenkovic, B. Bläsi, J. C. Goldschmidt, and M. Hermle, "Rear side sphere gratings for improved light trapping in crystalline silicon single junction and silicon-based tandem solar cells," *Sol. Energy Mater. Sol. Cells* **142**, 60–65 (2015).
15. A. Mellor, I. Tobias, A. Marti, M. J. Mendes, and A. Luque, "Upper limits to absorption enhancement in thick solar cells using diffraction gratings," *Prog. Photovoltaics* **19**(6), 676–687 (2011).
16. I. M. Peters, M. Rüdiger, H. Hauser, M. Hermle, and B. Bläsi, "Diffractive gratings for crystalline silicon solar cells-optimum parameters and loss mechanisms," *Prog. Photovoltaics* **20**(7), 862–873 (2012).
17. N. Tucher, J. Eisenlohr, P. Kiebel, O. Höhn, H. Hauser, I. M. Peters, C. Müller, J. C. Goldschmidt, and B. Bläsi, "3D optical simulation formalism OPTOS for textured silicon solar cells," *Opt. Express* **23**(24), A1720 (2015).
18. C. Haase and H. Stiebig, "Thin-film silicon solar cells with efficient periodic light trapping texture," *Appl. Phys. Lett.* **91**(6), 061116 (2007).
19. C. Rockstuhl, S. Fahr, K. Bittkau, T. Beckers, R. Carius, F.-J. Haug, T. Soderstrom, C. Ballif, and F. Lederer, "Comparison and optimization of randomly textured surfaces in thin-film solar cells," *Opt. Express* **18**(S3), A335–A342 (2010).
20. K. Bittkau, T. Beckers, S. Fahr, C. Rockstuhl, F. Lederer, and R. Carius, "Nanoscale investigation of light-trapping in a-Si:H solar cell structures with randomly textured interfaces," *Phys. Status Solidi A* **205**(12), 2766–2776 (2008).
21. E. R. Martins, J. Li, Y. Liu, V. Depauw, Z. Chen, J. Zhou, and T. F. Krauss, "Deterministic quasi-random nanostructures for photon control," *Nat. Commun.* **4**(1), 2665 (2013).
22. M.-C. van Lare and A. Polman, "Optimized Scattering Power Spectral Density of Photovoltaic Light-Trapping Patterns," *ACS Photonics* **2**(7), 822–831 (2015).
23. Y. Tanaka, Y. Kawamoto, M. Fujita, and S. Noda, "Enhancement of broadband optical absorption in photovoltaic devices by band-edge effect of photonic crystals," *Opt. Express* **21**(17), 20111–20118 (2013).
24. U. W. Paetzold, M. Smeets, M. Meier, K. Bittkau, T. Merdzhanova, V. Smirnov, D. Michaelis, C. Waechter, R. Carius, and U. Rau, "Disorder improves nanophotonic light trapping in thin-film solar cells," *Appl. Phys. Lett.* **104**(13), 131102 (2014).
25. S. Nanz, A. Abass, P. M. Piechulla, A. Sprafke, R. B. Wehrspohn, and C. Rockstuhl, "Strategy for tailoring the size distribution of nanospheres to optimize rough backreflectors of solar cells," *Opt. Express* **26**(2), A111 (2018).
26. P. M. Piechulla, L. Muehlenbein, R. B. Wehrspohn, S. Nanz, A. Abass, C. Rockstuhl, and A. Sprafke, "Fabrication of Nearly-Hyperuniform Substrates by Tailored Disorder for Photonic Applications," *Adv. Opt. Mater.* **6**(7), 1701272 (2018).
27. G. R. Strobl, *The Physics of Polymers. Concepts for understanding their structures and behavior*. Concepts for Understanding Their Structures and Behavior, 3rd rev. and expanded ed. (Springer-Verlag Berlin, Heidelberg, New York; Springer, 2007).
28. S. Walheim, M. Böltau, J. Mlynek, G. Krausch, and U. Steiner, "Structure Formation via Polymer Demixing in Spin-Cast Films," *Macromolecules* **30**(17), 4995–5003 (1997).
29. C. Ton-That, A.G. Shard, and R. H. Bradley, "Surface feature size of spin cast PS/PMMA blends," *Polymer* **43**(18), 4973–4977 (2002).
30. R. H. Siddique, Y. J. Donie, G. Gomard, S. Yalamanchili, T. Merdzhanova, U. Lemmer, and H. Hölscher, "Bioinspired phase-separated disordered nanostructures for thin photovoltaic absorbers," *Sci. Adv.* **3**(10), e1700232 (2017).
31. Y. J. Donie, M. Smeets, A. Egel, F. Lentz, J. B. Preinfalk, A. Mertens, V. Smirnov, U. Lemmer, K. Bittkau, and G. Gomard, "Light trapping in thin film silicon solar cells via phase separated disordered nanopillars," *Nanoscale* **10**(14), 6651–6659 (2018).
32. C. Huang, *Phase Separation in Thin Polymer Films: From Self Stratification to Polymer Blend Lithography*, Dissertation, TU Darmstadt, 2014.
33. O. Höhn, H. Hauser, N. Tucher, R. Müller, and B. Bläsi, "Modeling and realization of photonic structures for silicon-based tandem solar cells," in *Physics, Simulation, and Photonic Engineering of Photovoltaic Devices IX* (SPIE, 2020), p. 1.
34. M. J. Kerr, A. Cuevas, and R. A. Sinton, "Generalized analysis of quasi-steady-state and transient decay open circuit voltage measurements," *J. Appl. Phys.* **91**(1), 399–404 (2002).
35. F. Feldmann, C. Reichel, R. Müller, and M. Hermle, "The application of poly-Si/SiO_x contacts as passivated top/rear contacts in Si solar cells," *Sol. Energy Mater. Sol. Cells* **159**, 265–271 (2017).
36. D. Nečas and P. Klapetek, "Gwyddion," <http://gwyddion.net/documentation/user-guide-en/statistical-analysis.html#functions>.
37. ASTM G173-03, *Tables for Reference Solar Spectral Irradiances: Direct Normal and Hemispherical on 37 Tilted Surface*, 2012.
38. A. Vital, M. Vayer, T. Tilocher, R. Dussart, M. Boufnichel, and C. Sinturel, "Morphology control in thin films of PS:PLA homopolymer blends by dip-coating deposition," *Appl. Surf. Sci.* **393**, 127–133 (2017).
39. S. Song, K. T. Lee, C. W. Koh, H. Shin, M. Gao, H. Y. Woo, D. Vak, and J. Y. Kim, "Hot slot die coating for additive-free fabrication of high performance roll-to-roll processed polymer solar cells," *Energy Environ. Sci.* **11**(11), 3248–3255 (2018).